



OPEN A novel dynamic vibration absorber for vibration control of piping systems under multi-frequency harmonic excitations

Lihang Yin^{1,2}, Wei Xu^{1,2}, Zechao Hu^{1,2}✉ & Liantao Xiao^{1,2}

To suppress the significant vibration line spectra of piping systems under multi-frequency harmonic excitations, a novel dynamic vibration absorber (NDVA) is designed. The NDVA integrates numerous independent resonant units within a finite space through an ingenious structural design and possesses rich frequency regulation characteristics. A vibration model of the piping system equipped with the NDVA is established, and the approximate equivalent parameters of both the piping and the resonant units are inverted based on the frequency response function (FRF) test results. These parameters can be substituted into the model to enhance the accuracy and validity of the theoretical calculations. Based on the relationship between the absorbing bandwidth of the NDVA and the intervals of multi-frequency excitation frequencies, a tailored regulation strategy for different densities of excitation frequencies is proposed. Subsequently, the multi-frequency vibration reduction capability of the NDVA is verified through an example involving dual-frequency harmonic excitations. When there is a notable difference in the intensities of the multi-frequency vibration line spectra, a genetic algorithm is utilized to optimize the mass allocation of the resonant units. Simulation and test results demonstrate that the maximum response amplitude of the optimized system is further reduced.

Keywords Piping systems, Novel dynamic vibration absorber, Multi-frequency harmonic excitations, Regulation strategy, Mass allocation

Piping systems are important engineering structures that are widely used in the fields of ocean engineering, mechanical engineering, civil engineering, aerospace, and petrochemicals^{1,2}. Subjected to the combined effects of external excitation and internal fluid flow, piping systems are prone to exhibiting multi-frequency vibration line spectra^{3,4}. Strong vibrations in piping systems can lead to machine downtime, fatigue failure, fluid leakage, and even catastrophic explosions⁵.

Active control technologies use suitable control strategies to adjust the magnitude of the active force generated by the actuator in real time, thereby suppressing the vibration line spectra^{6,7}. Blocka et al.⁸ designed an annular hoop-type active control device to suppress fluid pulsations in a piping system, reducing the controlled pulsation line spectra by about 10–15 dB. Cheer et al.⁹ designed a similar active control structure, which reduced fluid pulsation in the piping but amplified vibrations near the location of the extruded pipe wall. However, the current active control technologies still suffer from high costs, complex control algorithms, and the need for numerous additional devices.

Dynamic vibration absorbers (DVAs) are commonly used for low-frequency vibration control. By adding auxiliary mass, spring, and damping to the main system, the additional system generates a reactive force^{10,11}. Shemshadi et al.¹² designed a cantilever beam DVA for piping vibration suppression, and the test results showed that the absorber had a positive vibration absorption effect at the excitation frequency. However, when the source vibration frequency shifts, the vibration absorption effect of conventional passive DVAs with fixed parameters is significantly reduced due to detuning^{13,14}. Therefore, they are generally used to suppress vibrations generated by single-frequency excitation.

To suppress multi-frequency excitations, Cunefare et al.¹⁵ proposed a state-switched absorber (SSA), which can change the absorbing frequency by switching its stiffness state during operation. Holdhusen¹⁶ utilized magneto-rheological elastomers to fabricate a SSA for vibration control of continuous system such as beams and plates, and the results showed that the SSA had better vibration reduction effects than conventional DVAs over

¹Institute of Noise and Vibration, Naval University of Engineering, Wuhan 430033, China. ²National Key Laboratory on Ship Vibration & Noise, Wuhan 430033, China. ✉email: huzechao68@outlook.com

a wider frequency band. However, the SSA requires frequent switching of stiffness states under multi-frequency excitations, which will reduce the service life of the SSA. Mani et al.¹⁷ developed an adaptive DVA for vibration reduction in piping systems using springs made of memory alloy. By changing the temperature, the Young's modulus of the memory alloy spring can be adjusted, thereby regulating the natural frequency of the absorber. However, adaptive DVAs have high requirements for control algorithms, and there may be a time delay when adjusting the stiffness of the absorber.

Igusa et al.¹⁸ proposed the multiple dynamic vibration absorber (MDVA), which can overcome the narrowband limitation of a single absorber by mounting several different absorbers on the main structure. Kashina et al.¹⁹ used a set of undamped resonators to reduce longitudinal or flexural waves in beams and derived relations for the optimum mass and number of the resonators required to achieve a certain attenuation over a specified frequency band. Yang et al.²⁰ explored the effect of the MDVA on vibration control of beam-type structures and calculated the optimal design parameters for each vibration absorber. However, the size and mass of each DVA in the conventional MDVA are usually large, and it is difficult to install a large number of DVAs in a limited space, which may hinder the richness of frequency regulation of the MDVA²¹.

In this paper, a novel dynamic vibration absorber (NDVA) is proposed, which integrates a large number of resonant units within a limited space through an ingenious structural design. Each resonant unit acts as an independent vibration absorber, and its frequency is adjusted by means of a variable mass, so that the NDVA can be flexibly adjusted to target single or multiple frequencies. To better cope with various multi-frequency harmonic excitation situations, we focus on the following two issues: (1) regulation strategy of the NDVA. Adopt a targeted frequency regulation strategy for resonant units based on the relationship between the density of excitation frequencies and the absorption bandwidth of the NDVA; (2) mass allocation of the NDVA. Reasonably deploy the mass distribution of resonant units based on the amplitude of the multi-frequency response, so that the NDVA can exhibit differential vibration reduction ability for different vibration line spectra, thereby enhancing its multi-frequency vibration reduction capability.

This paper is organized as follows: "Model" section introduces the structural and discrete models of the NDVA; "Response characteristics of the piping under multi-frequency harmonic excitations" section derives the frequency response function (FRF) and vibration response of the system under multi-frequency harmonic excitations, and determines the approximate equivalent parameters of the piping system and the resonant unit through a FRF test; "Frequency regulation strategy for the NDVA" section proposes frequency regulation strategy for the NDVA under dense and non-dense multi-frequency excitations; "Optimization of the NDVA under different multi-frequency excitation intensities" section uses a genetic algorithm to optimize the mass allocation of the resonant units under different multi-frequency response amplitudes, and conducts a multi-frequency excitations test to verify the optimization results; Some conclusions are given in "Conclusions" section.

Model

The diagram of the NDVA installed on the piping is shown in Fig. 1a. The NDVA mainly consists of a framework, resonant units and a mounting fixture. As a supporting structure, the framework is machined with three layers of circular holes arranged in a cyclic pattern. The resonant units can be divided into large resonant units (LRUs), medium resonant units (MRUs), and small resonant units (SRUs) according to their size. The SRUs, the LRUs, and the MRUs are respectively embedded within the inner, middle, and outer circular holes, as illustrated in Fig. 1b. The resonant unit is comprised of an elastic element, a basic mass, and an added mass. The elastic element relies on a short beam connecting the inner and outer rings to provide stiffness, while the added mass is attached to the basic mass, as shown in Fig. 1c. The mounting fixture, which includes hoops, connecting studs, and sleeves, is used to fix the NDVA on the piping. Because of the weak coupling between the resonant units within each layer, during the theoretical analysis of the NDVA, we can simplify the resonant units in each layer as a discrete spring-oscillator model, as depicted in Fig. 1d.

Response characteristics of the piping under multi-frequency harmonic excitations FRF of the piping system

After attaching the NDVA to the piping system, the FRF of the coupling system will be influenced by the impedance characteristics of the NDVA. We select one of the layers of the resonant units for analysis and derive the mechanical impedance, and the analysis process for resonant units in other layers is similar. Figure 2 presents the discrete model of the resonant unit, illustrating its two states when arranged vertically and obliquely. We define a global coordinate system x - o - y and a local coordinate system x_n - o - y_n ; m_n is the mass of the n -th vertical resonant unit; k_{nx} and k_{ny} are the spring stiffness in the x and y directions; c_{nx} and c_{ny} are the damping coefficient in the x and y directions, which can be calculated using formulas $c_{nx} = 2\zeta\sqrt{k_{nx}m_n}$ and $c_{ny} = 2\zeta\sqrt{k_{ny}m_n}$, respectively. Here, ζ denotes the damping ratio of the resonant unit, assuming that the damping ratios of all resonant units are the identical. θ_n is the rotation angle. When the resonant unit is placed obliquely, the parameter values of the mass, the spring stiffness and the damping coefficient remain unchanged, but the analytical coordinate system shifts from the global coordinate system to the local coordinate system. The oblique resonant unit exhibits a bending mode in the x_n direction and a tensile mode in the y_n direction.

The impedance of the n -th vertical resonant unit in the x and y directions can be expressed as:

$$Z_{nx}(\omega) = \frac{-\omega^2 m_n (k_{nx} + j\omega c_{nx})}{k_{nx} + j\omega c_{nx} - \omega^2 m_n}, Z_{ny}(\omega) = \frac{-\omega^2 m_n (k_{ny} + j\omega c_{ny})}{k_{ny} + j\omega c_{ny} - \omega^2 m_n} \quad (1)$$

where ω is the excitation frequency, assuming that the excitation frequencies in the x and y directions are the same.

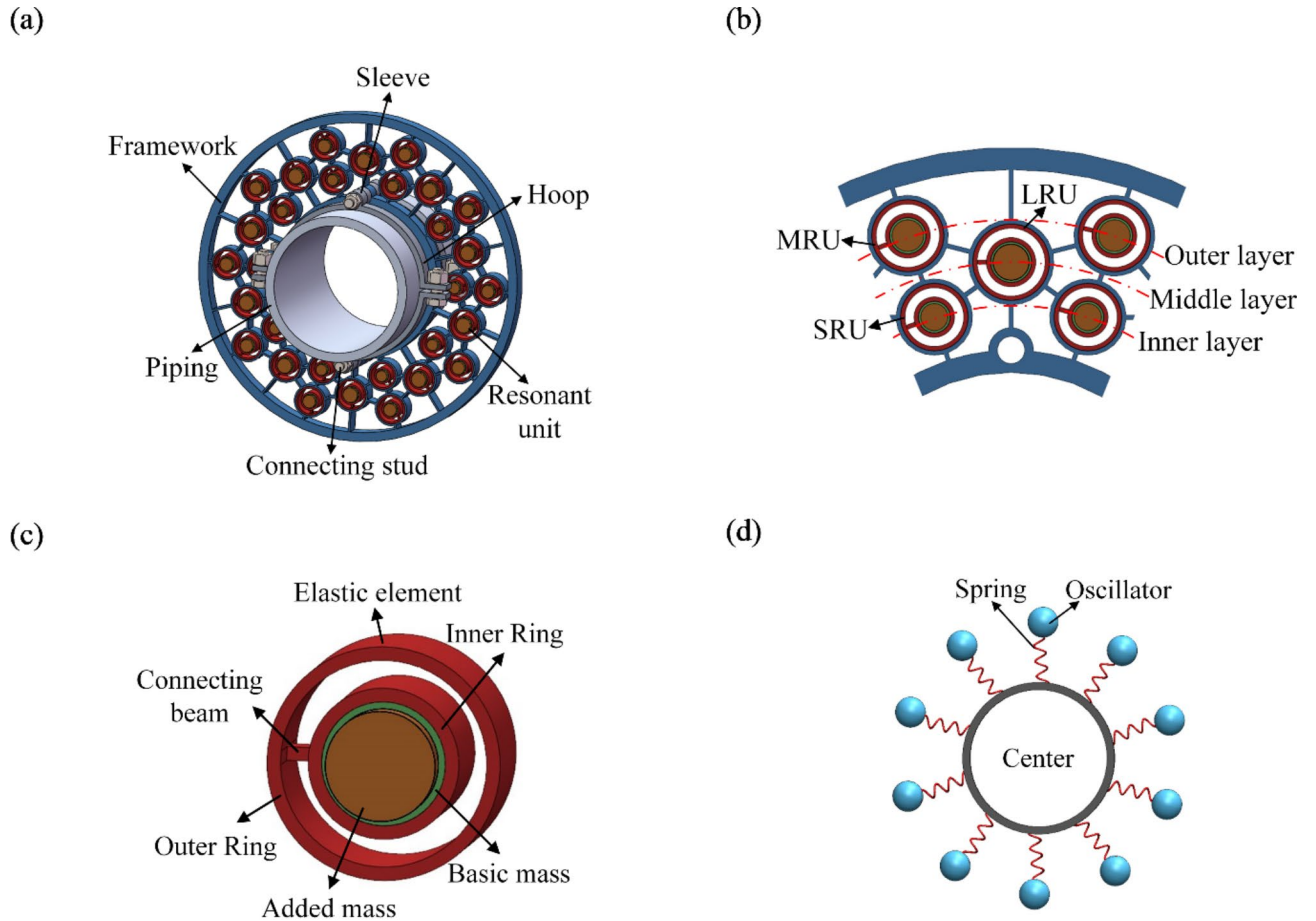


Fig. 1. Structural model of the NDVA. (a) diagram of the NDVA installed on the piping. (b) diagram of the resonant units embedded in the framework (c) diagram of the resonant unit. (d) diagram of the discrete model.

When the rotation angle is θ_n , the impedance of the resonant unit can be written as:

$$\mathbf{Z}_n(\omega) = \begin{bmatrix} \cos \theta_n & -\sin \theta_n \\ \sin \theta_n & \cos \theta_n \end{bmatrix} \begin{bmatrix} Z_{nx}(\omega) & 0 \\ 0 & Z_{ny}(\omega) \end{bmatrix} \begin{bmatrix} \cos \theta_n & -\sin \theta_n \\ \sin \theta_n & \cos \theta_n \end{bmatrix}^{-1} \quad (2)$$

Equation (2) can be further organized as:

$$\mathbf{Z}_n(\omega) = \begin{bmatrix} Z_{nx}(\omega) \cos^2 \theta_n + Z_{ny}(\omega) \sin^2 \theta_n & (Z_{nx}(\omega) - Z_{ny}(\omega)) \sin \theta_n \cos \theta_n \\ (Z_{nx}(\omega) - Z_{ny}(\omega)) \sin \theta_n \cos \theta_n & Z_{nx}(\omega) \sin^2 \theta_n + Z_{ny}(\omega) \cos^2 \theta_n \end{bmatrix} \quad (3)$$

Substitute Eq. (1) into Eq. (3) and list the diagonal elements of the total impedance matrix when the total number of the resonant units is S :

$$\begin{aligned} Z_{xx}(\omega) &= \sum_{n=1}^S \left(\frac{-\omega^2 m_n (k_{nx} + j\omega c_{nx})}{k_{nx} + j\omega c_{nx} - \omega^2 m_n} \cos^2 \theta_n + \frac{-\omega^2 m_n (k_{ny} + j\omega c_{ny})}{k_{ny} + j\omega c_{ny} - \omega^2 m_n} \sin^2 \theta_n \right) \\ Z_{yy}(\omega) &= \sum_{n=1}^S \left(\frac{-\omega^2 m_n (k_{nx} + j\omega c_{nx})}{k_{nx} + j\omega c_{nx} - \omega^2 m_n} \sin^2 \theta_n + \frac{-\omega^2 m_n (k_{ny} + j\omega c_{ny})}{k_{ny} + j\omega c_{ny} - \omega^2 m_n} \cos^2 \theta_n \right) \end{aligned} \quad (4)$$

where the impedance component $Z_{ab}(\omega)$ represents the ratio of the force in the a direction to the displacement response in the b direction, $a, b \in \{x, y\}$.

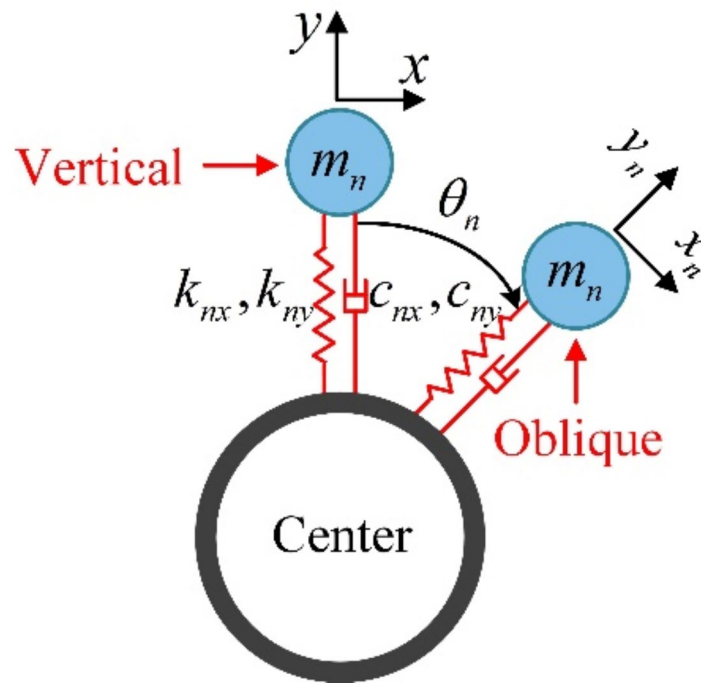


Fig. 2. Discrete model of the resonant unit.

According to Eq. (4), when the resonant unit is arranged obliquely, the impedance component of the NDVA is influenced by both the bending and tensile modes of the resonant unit. The tensile mode frequency of the resonant unit designed in this paper is significantly higher than the bending mode frequency. Therefore, utilizing the bending mode of the resonant unit as an effective vibration reduction mode for the NDVA is more beneficial for low-frequency vibration reduction. At this point, the tensile mode has minimal impact on the impedance of the NDVA.

Steady-state response of the system

Taking the excitation in the y direction as an example, assume that the multi-frequency harmonic excitations can be expressed as follows:

$$F = F_1 \sin(\omega_1 t + \phi_1) + F_2 \sin(\omega_2 t + \phi_2) + \dots + F_N \sin(\omega_N t + \phi_N) = F_i \sin(\omega_i t + \phi_i) \quad (5)$$

where F_i is the excitation amplitude; ω_i is the excitation frequency; ϕ_i is the excitation phase; i is the serial number of the harmonic excitation, $i = 1, 2, \dots, N$; N is the total number of the harmonic excitations.

The FRF of the piping system with the NDVA installed can be expressed as follows:

$$H(\omega) = \frac{1}{H_s^{-1}(\omega) + Z_{yy}(\omega)} \quad (6)$$

where $H_s(\omega)$ represents the vertical FRF of the original piping system.

According to the superposition principle, the steady-state response of the original piping system is:

$$q_s(t) = \sum_{i=1}^N |H_s(\omega_i)| F_i \sin(\omega_i t + \phi_i + \varphi_{si}) \quad (7)$$

where $\varphi_{si} = \arg(H_s(\omega_i))$ is the phase angle of the FRF of the original piping system at the i -th excitation frequency ω_i .

Then the steady-state response of the coupled system can be found:

$$q(t) = \sum_{i=1}^N |H(\omega_i)| F_i \sin(\omega_i t + \phi_i + \varphi_i) \quad (8)$$

where $\varphi_i = \arg(H(\omega_i))$ is the phase angle of the FRF of the coupled system at the i -th excitation frequency ω_i .

Equations (7) and (8) can be discretized as:

$$q_s(p) = \sum_{i=1}^N |H_s(\omega_i)| F_i \sin(\omega_i p T_{step} + \phi_i + \varphi_{si}) \quad (9)$$

$$q(p) = \sum_{i=1}^N |H(\omega_i)| F_i \sin(\omega_i p T_{step} + \phi_i + \varphi_i) \quad (10)$$

where T_{step} is the discrete time step and p is a positive integer.

FRF test

To improve the accuracy and practicability of the theoretical model, we conduct a FRF test to infer the equivalent parameters of the piping and the resonant units. These inferred parameters are then substituted into the theoretical model as input parameters, aiming to enhance its theoretical prediction capability. A piping test bench with elastic supports at both ends is constructed, and the NDVAs, acceleration sensors, and shaker are installed at the designated locations labeled in Fig. 3. A signal generator is utilized to produce a sweep excitation signal, which is amplified by a power amplifier to drive the shaker to apply vertical excitation. The diagram of the test setup is illustrated in Fig. 4.

The outer diameter of the piping in the test bench is 0.08 m, the wall thickness is 0.005 m, the length is 1.0 m, and the total mass is 3200 g. The mass of the framework is 165 g. The number of the resonant units per layer is 10. The added masses are round stainless steel sheets adapted to the dimensions of the resonant units. The masses of the resonant units are shown in Table 1, and the parameter configuration is based on our previous research work. The values in parentheses with italicized Arabic numerals in the table indicate the number of the resonant units at a given added mass thickness. The total mass of the coupled system after installing 4 NDVAs is calculated to be 5340 g.

For vertical excitation, the following two test conditions are set up: (1) V1: set the oblique angle of all resonant units to 0° , and the NDVA is adjusted to the non-absorbing direction, which only exerts the mass effect, so this condition is also used as a comparative condition; (2) V2: set the oblique angle of all resonant units to 90° , and the NDVA is adjusted to the absorbing direction. Figure 5 provides a schematic diagram of the arrangement of the resonant units under V1 and V2 conditions, showing the local area of the framework and clearly demonstrating

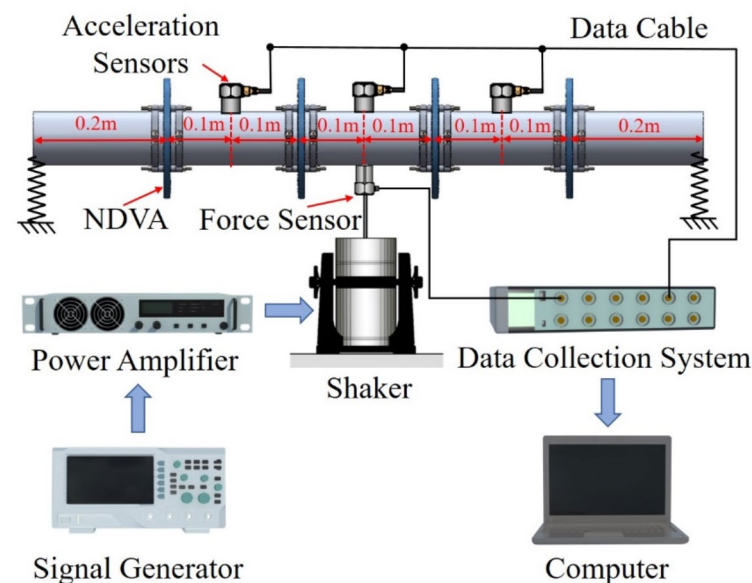


Fig. 3. Diagram of the excitation test process.

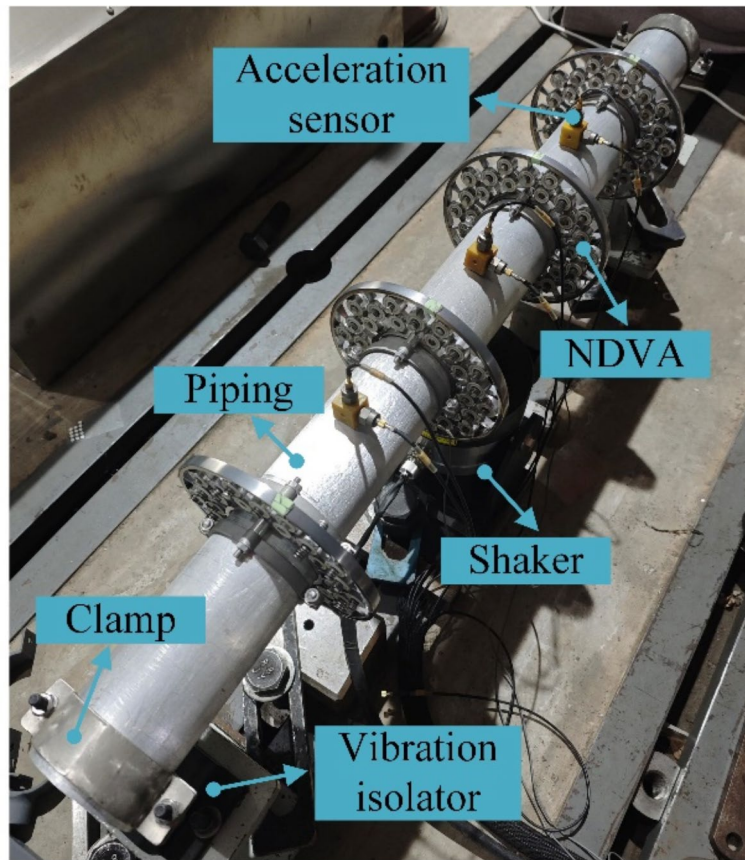


Fig. 4. Diagram of the test setup.

Parameters	Basic mass (g)	Added mass density (Calculated by thickness, g/mm)	Added mass thickness (mm)	Total mass (g)
LRU	12.2	0.40	12 (<i>10</i>)	17.0
MRU	9.7	0.30	7 (<i>10</i>)	11.8
SRU	7.4	0.22	4 (<i>10</i>)	8.3

Table 1. Mass of the resonant units in each NDVA during the FRF test. The number of the resonant units at a given added mass thickness is in [italics].

the arrangement status of the LRUs, the MRUs, and the SRUs. Then, The FRFs of the piping system under these two working conditions are measured.

The original piping is simplified to a centralized parameter system. Based on the test results under V1 condition, the approximate equivalent stiffness $k_s = 4.05e6$ N/m and damping ratio $\zeta_s = 0.015$ of the piping system can be derived. Based on the test results under V2 condition, the equivalent stiffness of the LRU, the MRU, and the SRU is derived as $k_{Leq} = 4.05e3$ N/m, $k_{Meq} = 4.15e3$ N/m, and $k_{Seq} = 3.85e3$ N/m, respectively. The damping ratio of the three resonant units is $\zeta = 0.045$. Figure 6 shows the comparison between the theoretical and test results of the FRF. It can be seen that the theoretical values are slightly lower than the test values overall, but the curves have similar trends, reflecting the accuracy of the theoretical model.

Frequency regulation strategy for the NDVA

Dual-frequency harmonic excitations constitute the simplest form of multi-frequency harmonic excitations. The literature^{10,22} extends the conclusions obtained from the analysis of dual-frequency harmonic excitations to the case of multi-frequency harmonic excitations. As a result, dual-frequency harmonic excitations are chosen for further analysis in the subsequent sections of the research. We believe that these analytical findings are equally applicable to the broader context of multi-frequency harmonic excitations.

The NDVA incorporates a substantial quantity of the resonant units, inevitably leading to natural mistuning during practical processing. This results in the eigenvalue splitting phenomenon, thereby enabling the NDVA to achieve a broad vibration absorption band²³. The absorption bandwidth of the NDVA can be expressed as $B = 2\zeta f_t$ (where f_t is the center frequency)²⁴. Due to the randomness of the natural mistuning of the resonant

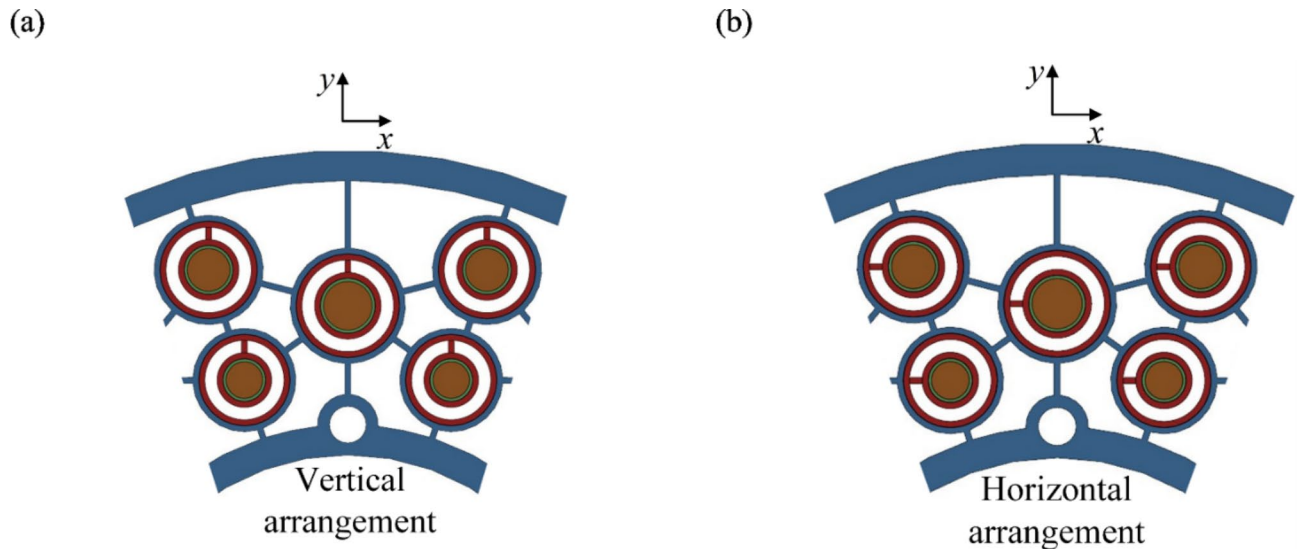


Fig. 5. Schematic diagram of the arrangement of the resonant units. **(a)** the arrangement of the resonant units under V1 condition. **(b)** the arrangement of the resonant units under V2 condition.

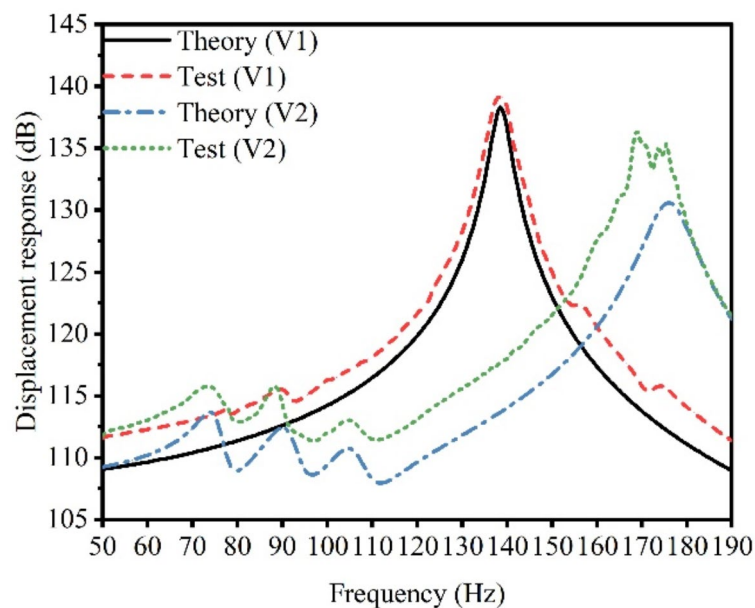


Fig. 6. Comparison of the theoretical and test results of the FRF.

units, it is assumed that the upper limit frequency f_{tu} , the lower limit frequency f_{lu} , and the center frequency f_t of the absorption frequency band satisfy $f_{tu} + f_{lu} = 2f_t$.

In Fig. 7a, the excitation frequency interval Δ_{f_F} is narrower than the bandwidth of the single-frequency NDVA, indicative of a dense multi-frequency excitations situation, where a significant multi-frequency vibration reduction effect can be accomplished using just the single-frequency NDVA. In Fig. 7b, Δ_{f_F} is wider than the bandwidth of the single-frequency NDVA, indicative of a non-dense multi-frequency excitations situation, where the effectiveness of the single-frequency NDVA in controlling the multi-frequency vibration line spectra becomes limited. Hence, it is imperative to regulate the number of the resonant frequencies to correspond with the number of the excitation frequencies, and to match the resonant frequencies as closely as possible with the excitation frequencies.

To verify the effectiveness of the regulation strategy, examples are designed to analyze the vibration absorption effect of the NDVA under different frequency densities of excitations. The design frequencies of the resonant units are adjusted to 91.0 Hz according to the mass allocation of method 1 in Table 2, and the bandwidth of the

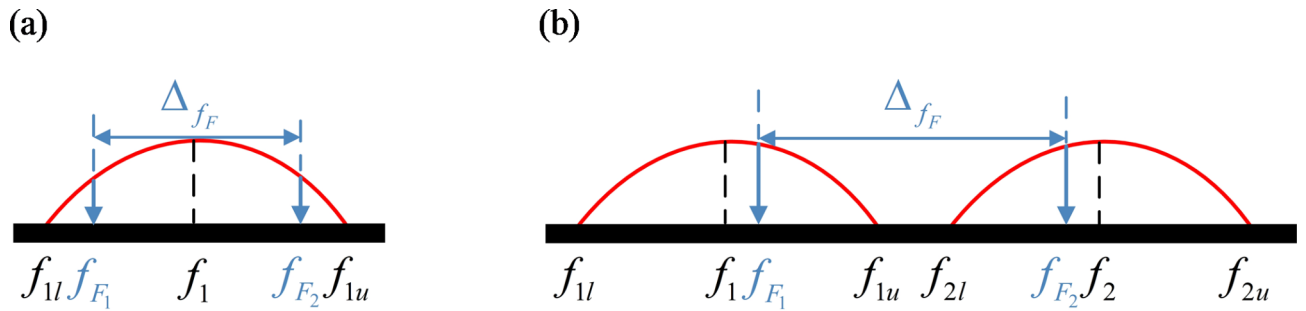


Fig. 7. Schematic of the frequency regulation of the NDVA. **(a)** the frequency regulation under dense multi-frequency excitations. **(b)** the frequency regulation under non-dense multi-frequency excitations.

Parameters		Basic mass (g)	Added mass (g)	Design frequency (Hz)
Method 1	LRU	12.2	0.3 (<i>10</i>)	90.5
	MRU	9.7	3.0 (<i>10</i>)	90.9
	SRU	7.4	4.4 (<i>10</i>)	90.9
Method 2	LRU	12.2	1.0 (<i>10</i>)	88.1
	MRU	9.7	3.9 (<i>5</i>); 2.2 (<i>5</i>)	87.9; 93.9
	SRU	7.4	3.6 (<i>10</i>)	94.1
Method 3	LRU	12.2	2.0 (<i>10</i>)	85.0
	MRU	9.7	4.8 (<i>1</i>); 1.9 (<i>9</i>)	85.1; 95.1
	SRU	7.4	3.4 (<i>10</i>)	95.0

Table 2. Parameter settings of the resonant units under different methods. The number of the resonant units at a given added mass is in [italics].

Forms of excitations	Excitation frequency (Hz)	Excitation amplitude (N)	Phase
Dense excitations	$f_{F_1} = 88.0; f_{F_2} = 94.0;$	$F_1 = F_2 = 1.0$	$\phi_1 \neq \phi_2$
Non-dense excitations	$f_{F_1} = 85.0; f_{F_2} = 95.0;$	$F_1 = F_2 = 1.0$	$\phi_1 \neq \phi_2$

Table 3. Parameter settings for different multi-frequency excitations.

NDVA is calculated to be 8.2 Hz. Two different excitation parameters are set in Table 3, which can simulate dense and non-dense multi-frequency excitations cases.

For both dense and non-dense multi-frequency excitation situations, set the LRUs and the SRUs to have only one resonant frequency, and set the MRUs to have multiple resonant frequencies. Allocate the mass of the resonant units according to methods 2 and 3 in Table 2. The resonant unit frequencies match the excitation frequencies, and the total mass of the NDVA under the three different methods in Table 2 remains roughly the same.

Figure 8 shows the time-domain responses of the piping system under dense dual-frequency harmonic excitations controlled by methods 1 and 2. It can be seen that, under dense dual-frequency excitations, the vibration reduction effect of the NDVA on the piping is similar in both methods.

Figure 9 illustrates the frequency-domain responses of the piping system under dense dual-frequency harmonic excitations, controlled by methods 1 and 2. It can be seen that by using the single-frequency NDVA, the response amplitude of the system is reduced from 4.0×10^{-7} m to 3.0×10^{-7} m at 88 Hz and from 4.7×10^{-7} m to 1.6×10^{-7} m at 94 Hz. In contrast, with the dual-frequency NDVA, the response amplitude is reduced to 2.7×10^{-7} m at 88 Hz and 1.9×10^{-7} m at 94 Hz. Evidently, under dense multi-frequency harmonic excitations, the NDVA's broadband vibration absorbing capability can be effectively harnessed to achieve a superior control outcome, thereby simplifying the challenge of the frequency regulation.

Figure 10 depicts the time-domain responses of the piping system under non-dense dual-frequency harmonic excitations, controlled by methods 1 and 3. Notably, in scenarios involving non-dense dual-frequency excitations, the vibration reduction effect of the dual-frequency NDVA surpasses that of the single-frequency NDVA significantly.

Figure 11 shows the frequency-domain responses of the piping system under non-dense dual-frequency harmonic excitations, controlled by methods 1 and 3. It can be observed that by using the single-frequency NDVA, the response amplitude of the system increases from 4.0×10^{-7} to 6.5×10^{-7} m at 85 Hz, whereas it decreases from 4.7×10^{-7} to 1.6×10^{-7} m at 95 Hz. In contrast, with the dual-frequency NDVA, the

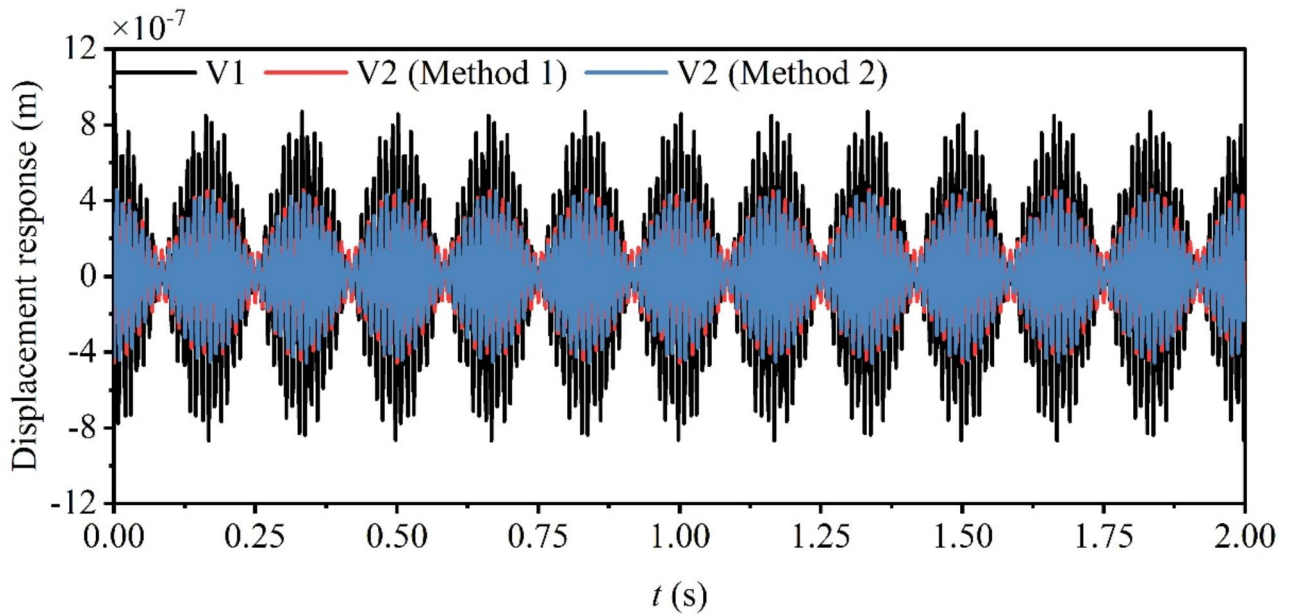


Fig. 8. Time-domain responses under dense dual-frequency harmonic excitations.

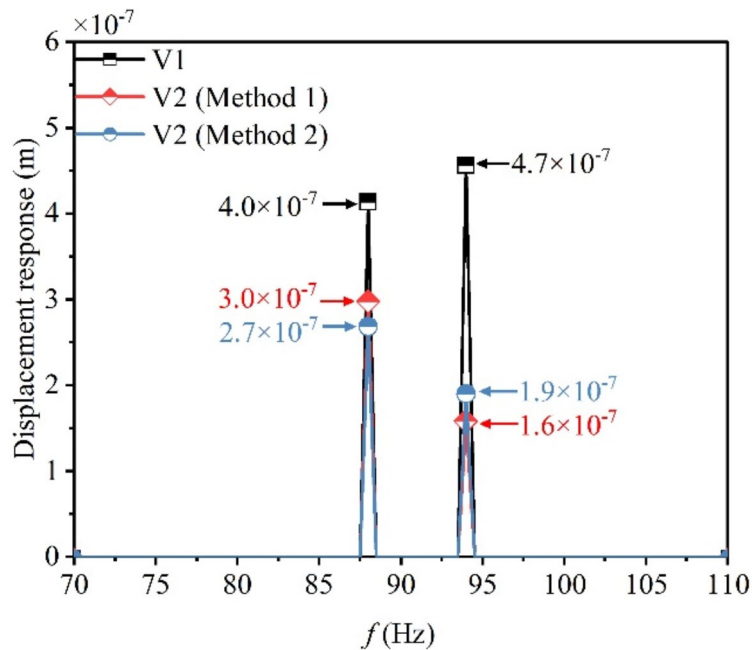


Fig. 9. Frequency-domain responses under dense dual-frequency harmonic excitations.

response amplitude is reduced to 3.4×10^{-7} m at 85 Hz and 2.0×10^{-7} m at 95 Hz. Evidently, under dense multi-frequency harmonic excitations, the vibration reduction capability of the single-frequency NDVA may be restricted, and in some cases, it may even amplify the vibration. However, adjusting the resonant frequencies to align with the excitation frequencies can substantially enhance the vibration reduction effectiveness.

Optimization of the NDVA under different multi-frequency excitation intensities Mass optimization allocation

The regulation strategy presented in "Frequency regulation strategy for the NDVA" section has demonstrated favorable effects on multi-frequency vibration reduction and can serve as a fundamental, straightforward, and efficient regulation approach. However, it does not account for the intensities of multi-frequency vibration line

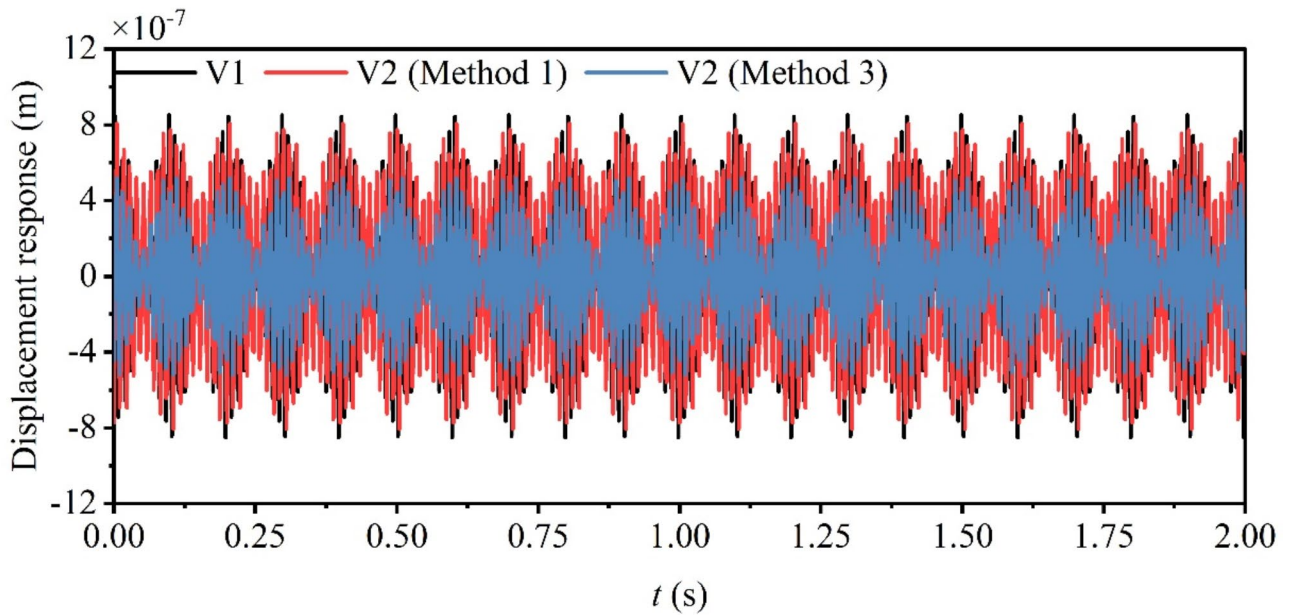


Fig. 10. Time-domain responses under non-dense dual-frequency harmonic excitations.

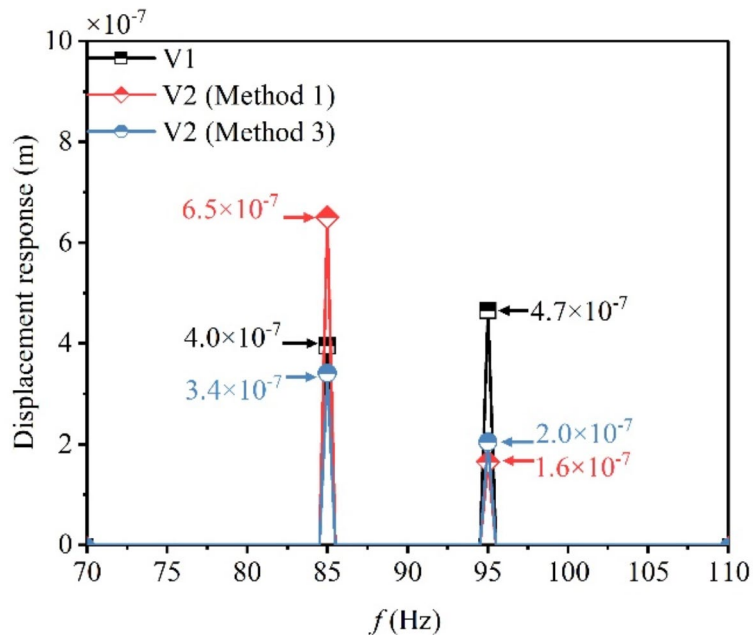


Fig. 11. Frequency-domain responses under non-dense dual-frequency harmonic excitations.

spectra. In reality, vibration line spectra with greater intensity contribute more to the overall vibration level of the system, which requires us to allocate more absorbing mass. In this section, we employ the genetic algorithm to optimize the mass allocation of each resonant unit under different multi-frequency excitation intensities, enabling the NDVA to exhibit differentiated absorption capabilities for response spectra of varying amplitudes.

The NDVA's extensive regulation capabilities allow for numerous mass allocation strategies. If the mass of each resonant unit is treated as an optimization variable, the multitude of optimization variables will significantly prolong the optimization process. To streamline the optimization, we limit the number of the adjustable frequencies for each type of the resonant unit to match the number of multi-frequency excitation frequencies. This not only drastically reduces the number of optimization variables but also ensures the richness of resonant unit frequency adjustment.

Option	Value	Option	Value
Sub-population size	10	Rate of migration	0.01
Number of islands	10	Interval of migration	5
Number of generations	20	Elite size	1
Rate of crossover	1.0	Rel tournament size	0.5
Rate of mutation	0.01		

Table 4. Optimization parameter settings for multi-island genetic algorithm.

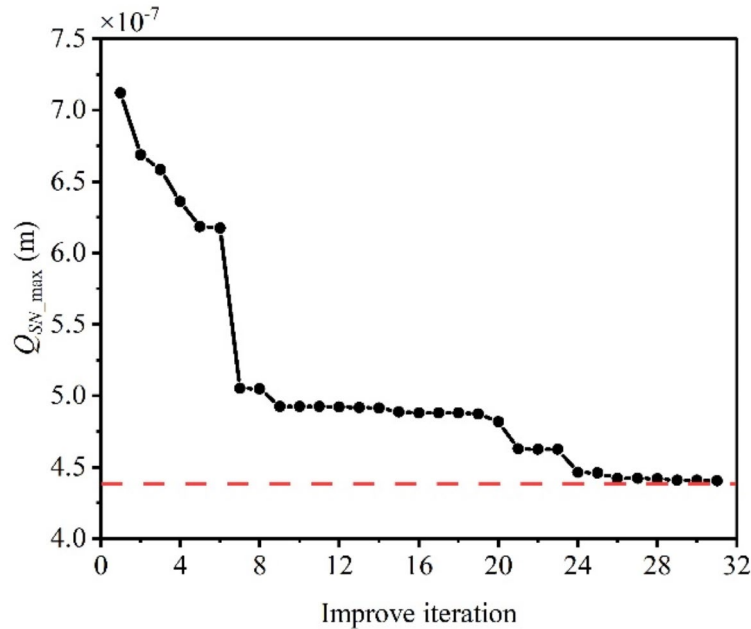


Fig. 12. Optimization iteration process.

Adjust the amplitudes of multi-frequency harmonic excitations in Table 3 to $F_1 = 2.0N$ and $F_2 = 1.0N$, respectively, while maintaining all other parameters unchanged. For the LRUs, denote the masses as m_{L1} and m_{L2} , with the corresponding number of the resonant units being N_{L1} and N_{L2} ; For the MRUs, denote the masses as m_{M1} and m_{M2} , with the corresponding number of the resonant units being N_{M1} and N_{M2} ; For the SRUs, denote the masses as m_{S1} and m_{S2} , with the corresponding number of the resonant units being N_{S1} and N_{S2} . Additionally, let e_m represent the absolute change in the total mass before and after the optimization of the resonant units. Fast Fourier Transform (FFT) is applied to the time-domain response signal, and let Q_{SN_max} represent the maximum magnitude of the frequency-domain response of the piping system with the NDVA attached.

Define the following optimization problem:

Optimization variables: $m_{L1}, m_{L2}, N_{L1}; m_{M1}, m_{M2}, N_{M1}; m_{S1}, m_{S2}, N_{S1}$.

Optimization objective: Minimize: Q_{SN_max} .

Constraints: $0 \leq N_{L1} \leq 10; 0 \leq N_{M1} \leq 10; 0 \leq N_{S1} \leq 10; 0 \leq e_m \leq 0.01$.

Optimization algorithm: multi-island genetic algorithm, whose optimization parameters are set as in Table 4.

Figure 12 illustrates the improvement iteration process of the multi-island genetic algorithm. It is observable that the optimization objective gradually stabilizes after numerous iterations, and the convergence of the optimization model is excellent.

The optimized variable parameter values are shown in Table 5.

The time-domain responses of the piping system with the NDVA attached before and after optimization are shown in Fig. 13. We can see that the time-domain responses undergo further reduction after optimization.

Following the application of FFT to the time-domain signal, the frequency-domain responses of the piping system can be obtained, as shown in Fig. 14. It is clear that after mass optimization allocation, the maximum amplitude of the multi-frequency vibration line spectra of the piping system is further reduced.

Parameters		Basic mass (g)	Added mass (g)	Added mass thickness (mm)
LRU	m_{L1}	12.2	2.2	6 (7)
	m_{L2}	12.2	2.4	6 (3)
MRU	m_{M1}	9.7	5.8	19 (8)
	m_{M2}	9.7	1.6	5 (2)
SRU	m_{S1}	7.4	1.2	5 (2)
	m_{S2}	7.4	0.3	1 (8)

Table 5. Parameters of optimized resonant units. The number of the resonant units at a given added mass thickness is in [italics].

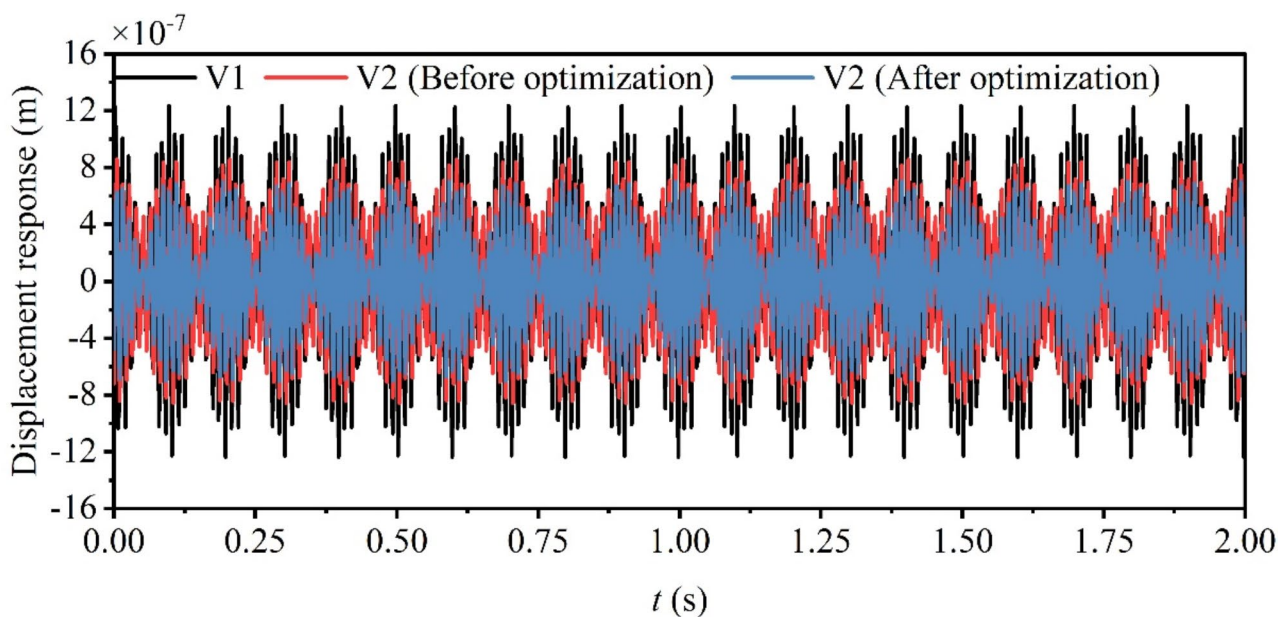


Fig. 13. Time-domain responses of the piping before and after mass optimization allocation.

Test verification

To verify the improvement of vibration reduction effect of the NDVA after mass optimization allocation, a dual-frequency harmonic excitations test is conducted on the bench shown in Fig. 4. Excitation signals are generated according to the parameters listed in Table 3, and a comparison of the frequency-domain vibration reduction performance of the NDVA, before and after optimal mass allocation, is undertaken. The test results are shown in Fig. 15.

It can be seen that the test results align closely with the theoretical predictions. When the NDVA is adjusted to the non-absorbing direction, the response amplitude at 85 Hz is 1.33×10^{-6} m, and the response amplitude at 95 Hz is 6.8×10^{-7} m. Alternatively, when the NDVA is adjusted to the absorbing direction, before mass optimization allocation, the response amplitude at 85 Hz exhibits an attenuation of 29.4%, while at 95 Hz, the attenuation is 45.3%; After mass optimization allocation, the NDVA allocates more mass to the vibration line spectrum at 85 Hz, increasing the amplitude attenuation to 45.2%. However, the response amplitude attenuation at 95 Hz decreases to 35.9%. After optimization, the maximum response amplitude of the system drops from 9.4×10^{-7} m to 7.3×10^{-7} m, indicating a further improvement in the vibration reduction effectiveness of the NDVA.

Conclusions

In this paper, the NDVA is proposed for suppressing multi-frequency responses in piping systems. It integrates a large number of resonant units within a finite space and possesses rich frequency regulation capabilities.

The vibration response model of the piping system with the NDVA attached is established, and the approximate equivalent parameters of the piping and the resonant units are derived based on the FRF test results. The theoretical results of the FRF align well with the test results, indicating the reliability of the theoretical model.

For dense multi-frequency excitations, a significant multi-frequency vibration reduction effect can be accomplished using a single-frequency NDVA alone, which can simplify the difficulty of frequency design and regulation of the NDVA. For non-dense multi-frequency excitations, it is imperative to regulate the number of

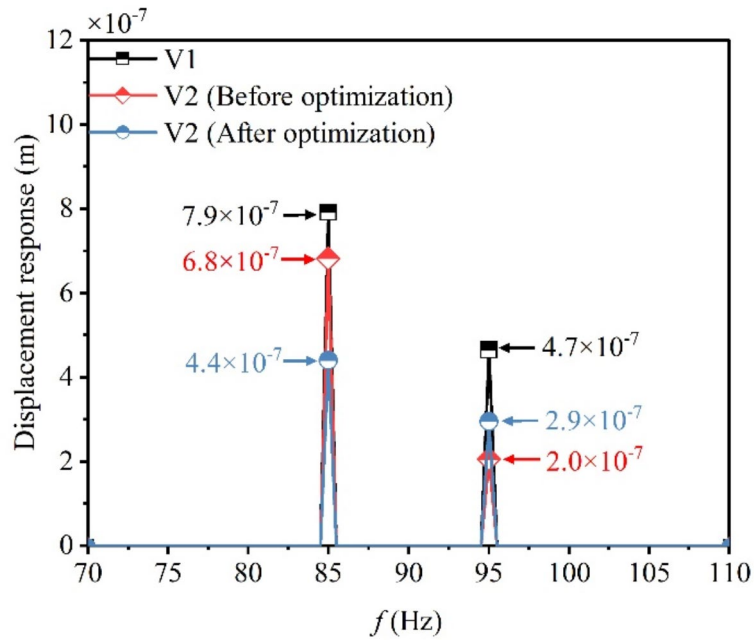


Fig. 14. Frequency-domain responses of the piping before and after mass optimization allocation.

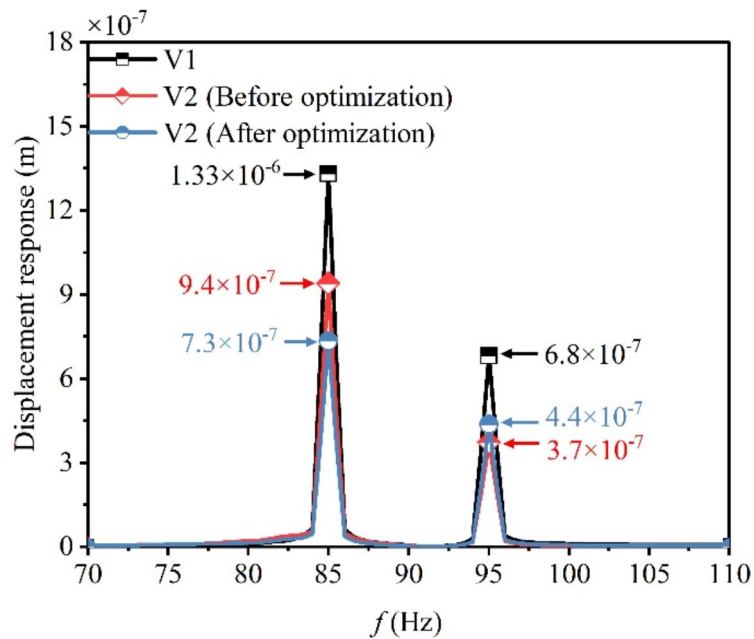


Fig. 15. Test results of the piping vibration before and after mass optimization allocation.

the resonant frequencies to correspond with the number of the excitation frequencies, while ensuring that the resonant frequencies match the excitation frequencies as closely as possible.

When there is a notable difference in the intensities of the multi-frequency vibration line spectra, the genetic algorithm is employed to redistribute the masses of the resonant units. A dual-frequency harmonic excitations test is conducted, and the results show that the maximum response amplitude in the frequency-domain of the piping system is reduced from 9.4×10^{-7} to 7.3×10^{-7} m, indicating a further improvement in the vibration reduction effectiveness of the NDVA.

Data availability

The data that support the findings of this study are available from the corresponding author upon reasonable request.

Received: 2 November 2024; Accepted: 8 January 2025

Published online: 15 January 2025

References

- Liang, X. et al. Semi-analytical solution for dynamic behavior of a fluid-conveying pipe with different boundary conditions. *Ocean Eng.* **163**, 183–190 (2018).
- Païdoussis, M. P. Pipes conveying fluid: A fertile dynamics problem. *J. Fluids Struct.* **114**, 103664 (2022).
- Ding, H., Ji, J. & Chen, L. Nonlinear vibration isolation for fluid-conveying pipes using quasi-zero stiffness characteristics. *Mech. Syst. Signal Process.* **121**, 675–688 (2019).
- Ji, W., Sun, W., Ma, H. & Li, J. Dynamic modeling and analysis of fluid-delivering cracked pipeline considering breathing effect. *Int. J. Mech. Sci.* **264**, 108805 (2024).
- Zheng, J. et al. Water hammer detection based on FIV online analysis using a distributed fiber optic sensor. *Appl. Opt.* **62**(28), 7455–7462 (2023).
- Zhang, Y., Sun, W., Zhang, H., Du, D. & Xu, K. Active vibration control of fluid-conveying pipelines: Theoretical and experimental studies. *Int. J. Mech. Sci.* **270**, 109106 (2024).
- Lin, Y. H. & Chu, C. L. Active flutter control of a cantilever tube conveying fluid using piezoelectric actuators. *J. Sound Vib.* **196**(1), 97–105 (1996).
- Blocka, C., Engelhardt, J. & Henkela, F. O. Active control of vibrations in piping systems. In *20th International Conference on Structural Mechanics in Reactor Technology (SMiRT 20)*. (Espoo 2009).
- Cheer, J. & Daley, S. Broadband active control of noise and vibration in a fluid-filled pipeline using an array of non-intrusive structural actuators. *INTER NOISE NOISE CON Congr. Conf. Proc.* **250**(3), 3492–3501 (2015).
- Sun, H. L., Zhang, P. Q., Chen, H. B., Zhang, K. & Gong, X. L. Application of dynamic vibration absorbers in structural vibration control under multi-frequency harmonic excitations. *Appl. Acoust.* **69**(12), 1361–1367 (2008).
- Gao, P., Xiang, C., Liu, H. & Zhou, H. Reducing variable frequency vibrations in a powertrain system with an adaptive tuned vibration absorber group. *J. Sound Vib.* **425**, 82–101 (2018).
- Shemshadi, M., Karimi, M. & Veysi, F. A simple method to design and analyze dynamic vibration absorber of pipeline structure using dimensional analysis. *Shock Vib.* **27**(2478371), 1–13 (2021).
- Li, H., Wu, S., Chen, Q. & Fei, Q. Design of dynamic absorbers to control the flexural resonant vibration of structures characterized by multiple natural modes. *J. Sound Vib.* **513**, 116415 (2021).
- Mane, P. U. & Kondekar, G. R. Experimental study on vibration control using shape memory alloy based vibration absorber. *Mater. Today Proc.* **45**, 2812–2817 (2021).
- Cunefare, K. A., Rosa, S. D., Sadegh, N. & Larson, G. State-switched absorber for semi-active structural control. *J. Intell. Mater. Syst. Struct.* **11**(4), 300–10 (2000).
- Holdhusen, M. H. The state-switched absorber used for vibration control of continuous systems. PhD thesis. Georgia Institute of Technology 2005.
- Mani, Y. & Senthilkumar, M. Shape memory alloy-based adaptive-passive dynamic vibration absorber for vibration control in piping applications. *J. Vib. Control* **21**(9), 1838–1847 (2013).
- Igusa, T. & Xu, K. Vibration control using multiple tuned mass dampers. *J. Sound Vib.* **175**(4), 491–503 (1994).
- Kashina, V. I. & Tyutekin, V. V. Waveguide vibration reduction of longitudinal and flexural modes by means of a multielement structure of resonators. *Soviet Phys. Acoust.* **36**(4), 383–85 (1990).
- Yang, F., Esmailzadeh, E. & Sedaghati, R. Optimal vibration control of beam-type structures using multiple-tuned-mass-dampers. *Proc. Instit. Mech. Eng. Part K J. Multi-body Dyn.* **224**(2), 191–202 (2009).
- Wang, X., Pang, Y., Hui, W. J. & Ma, F. A broadband metamaterial damper design based on synergetic coupling among multi-cells. *Appl. Acoust.* **206**, 109303 (2023).
- Zhang, J., Ding, H., Mao, X. & Chen, L. Multi-frequency harmonic balance method for nonlinear vibration of pipe conveying fluid under arbitrary dual-frequency excitation. *Nonlinear Dyn.* <https://doi.org/10.1007/s11071-024-10445-w> (2024).
- Liu, Z., Liu, W., Gao, W. & Cheng, X. Advances of research on mode localization in mistuned cyclically periodic structures. *Appl. Mech. Mater.* **405–408**, 3198–3203 (2013).
- Brennan, M. J. Characteristics of a wideband vibration neutralizer. *Noise Control Eng. J.* **45**(5), 201–207 (1997).

Acknowledgements

The authors are grateful for the financial support provided by National Major Science and Technology Project (Number: J2019-II-0013-0033) and National Defence Key Laboratory Foundation (Number: 6142204240305).

Author contributions

L.Y.: Conceptualization, Data curation, Software, Visualization, Writing—original draft. W.X.: Conceptualization, Investigation, Writing—review and editing. Z.H.: Conceptualization, Methodology, Writing—review and editing. L.X.: Writing—review and editing.

Declarations

Competing interests

The authors declare no competing interests.

Additional information

Correspondence and requests for materials should be addressed to Z.H.

Reprints and permissions information is available at www.nature.com/reprints.

Publisher's note Springer Nature remains neutral with regard to jurisdictional claims in published maps and institutional affiliations.

Open Access This article is licensed under a Creative Commons Attribution-NonCommercial-NoDerivatives 4.0 International License, which permits any non-commercial use, sharing, distribution and reproduction in any medium or format, as long as you give appropriate credit to the original author(s) and the source, provide a link to the Creative Commons licence, and indicate if you modified the licensed material. You do not have permission under this licence to share adapted material derived from this article or parts of it. The images or other third party material in this article are included in the article's Creative Commons licence, unless indicated otherwise in a credit line to the material. If material is not included in the article's Creative Commons licence and your intended use is not permitted by statutory regulation or exceeds the permitted use, you will need to obtain permission directly from the copyright holder. To view a copy of this licence, visit <http://creativecommons.org/licenses/by-nc-nd/4.0/>.

© The Author(s) 2025